Waveguide integration of a > 4.7-THz quantum-cascade laser

Eleanor Nuttall,[1] Yingjun Han,[1] Diego Pardo,[2] Sanchit S. Kondawar,[1] Nick Brewster,[2] Mohammed Salih,[1] Lianhe Li,[1] Michael D. Horbury,[1] A. Giles Davies,[1] Edmund H. Linfield,[1] Hui Wang,[2] Paul Dean,[1] Brian N. Ellison,[2] and Alexander Valavanis[1]

[1] *School of Electronic and Electrical Engineering, The University of Leeds, Leeds LS2 9JT, U.K.*

[2] *UKRI–STFC Rutherford Appleton Laboratory, Harwell Oxford, Didcot OX11 0QX, U.K.*

Email: cm14en@leeds.ac.uk

We have demonstrated waveguide integration of terahertz quantum cascade lasers (THz QCLs) at frequencies above 4.7 THz. A precision micromachining technique, followed by diamond-turning and electroless-plating has been used to manufacture hollow rectangular waveguides with integrated diagonal feedhorns. We show that surface roughness at the ~ 1 µm level is achieved, enabling outcoupling of radiation in the 4.75–5.05 THz band, with a divergence angle of <5° along the plane of the QCL substrate.

Introduction: Terahertz-frequency quantum-cascade lasers (THz QCLs) are compact, yet powerful semiconductor sources of radiation in the ~2–5-THz band of the electromagnetic spectrum [1]. These devices have a wide range of potential applications, including atmospheric and space research [2], security imaging [3] and biomedical analysis [4], owing to their high emission intensity, narrow intrinsic linewidths, and compact size. However, integration of THz QCLs with other system components is challenging, both in terms of near-field coupling to external waveguides, and far-field quasi-optical coupling to external devices.

The gain medium of a THz QCL consists of a stack of semiconductor layers, which are grown using molecular-beam epitaxy (MBE) to a total thickness of ~ 10 µm, and enclosed within a plasmonic waveguide structure. The electromagnetic mode profile across the laser facet is, therefore, considerably narrower than the ~ 100-µm free-space emission wavelength. This results in a widely divergent and non-Gaussian far-field beam pattern [5], which is challenging to couple into external devices. This can be mitigated partially, through a range of photonic engineering approaches and custom assemblies of quasi-optical components (e.g., Ref. [6]).

Alternatively, direct (near-field) coupling between components is a more attractive option for application environments, such as satellite payloads, in which the system volume, mass and mechanical robustness are key constraints. However, the dimensional tolerances required for manufacturing waveguides and the coupling interfaces become extremely challenging as the THz frequency of the source increases. Nevertheless, some progress has been made toward direct coupling between THz QCLs and other components. Monolithic semiconductor fabrication processes have been used to integrate 2.8-THz QCLs with Schottky mixers [7], and 3.4-THz QCLs with modulators [8]. We have also previously embedded 3.5-THz QCLs into precision micromachined metallic waveguides, which are optically out-coupled to either rectangular apertures [9] or diagonal feedhorns [10]. It is though, desirable to extend these approaches to exploit the highest achievable frequency range of QCLs, up to around ~5 THz. For example, 4.7-THz QCLs are required for radiometric observations of atomic oxygen [11], but this requires a 34% improvement in the machining tolerances to achieve comparable waveguide performance to that achieved at 3.5-THz.

In this work, we demonstrate the first such high-frequency waveguide integration of a QCL, emitting in the 4.7–5.1-THz band. We achieve this through a combination of precision milling, diamond-turned surface finishing, and electroless gold plating. Compared to standard gold plating, we have achieved an order-of-magnitude reduction in gold grain size to ~1 µm, enabling successful propagation and outcoupling of THz radiation (Figure 2). The following sections describe the fabrication of the QCL and its waveguide enclosure, and characterisation of its optical and thermal performance.

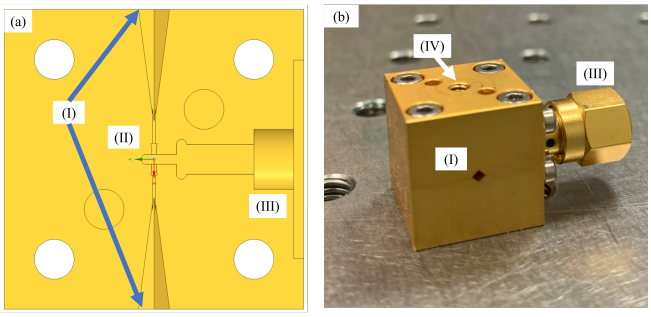

Fig 1 *Structure of QCL waveguide module, showing (a) top-down computer-aided-design rendering of the internal structure of the lower half-block, and (b) photograph of the exterior of the assembled module. Labels show (I) diagonal feedhorn apertures at either side of the waveguide channel, (II) QCL recess and waveguide channel, (III) SMA connector and internal bonding point, (IV) mounting point for external temperature probe.*

Device fabrication: The QCL active region was based on a ~4.7-THz GaAs/AlGaAs phonon-enhanced bound-to-continuum design [12], which was grown using molecular-beam epitaxy to a thickness of 12 µm. The device was then processed into a gold–gold double-metal plasmonic ridge-waveguide configuration, with a transverse ridge width of 60 µm, and with the substrate thickness reduced to 88 µm, using a combination of wet chemical etching and mechanical lapping processes. The device was cleaved to a length of 1200 µm, and diced using a diamond wafer-saw, to a chip of width ~200 µm.

An external waveguide enclosure with diagonal feedhorns was fabricated for the QCL, using a split-block machining approach [13]. This feedhorn geometry allows strong coupling of radiation into the fundamental Gaussian mode, while being much simpler to fabricate than structures such as corrugated conical feedhorns. A pair of oxygen-free copper blocks, each with base area of (15 × 15) mm^2 and a height of 7.5 mm were used to form the enclosure. Rectangular channels with widths and depths of 170 µm and 40 µm respectively were precision machined into each block, as shown in Figure 1(a) using a KERN mill. The two blocks were aligned using precision dowels, such that they co-registered to form a complete enclosure, containing a hollow rectangular waveguide with a cross-sectional area of (170 × 80) µm^2 [Figure 1(b)]. A diagonal feedhorn with an across-diagonal aperture of (1.56 × 1.56)-mm^2 was milled into each channel with a slant angle of 7.5°. An additional recessed area, with a 1600 µm length and 250 µm width, was milled into the centre of the lower channel, to house the QCL.

A set of surface-finishing steps was undertaken to achieve good performance at >4.7 THz. The surface of each block was finished using a Precitech Nanoform X™ single-point diamond turning lathe, to achieve a surface roughness on the scale of ~10 nm. The surfaces of the copper blocks were then finished with a gold electroless plating process, resulting in a gold grain size on the scale of ~ 1 µm. For comparison, an equivalent electroplating process was found to yield ~ 10 µm roughness, as shown in Figure 2. The QCL was solder-mounted into the recessed

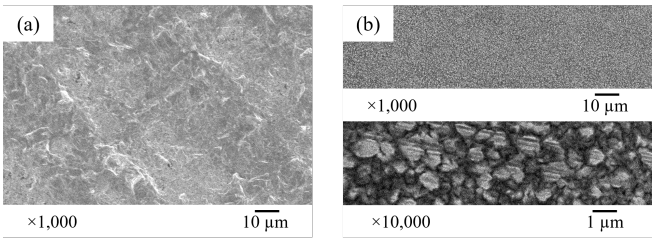

Fig 2 *Scanning electron micrographs of surface-finishing tests on oxygen-free copper, using (a) standard gold plating process at 1,000× magnification, and (b) electroless gold-plating and diamond turning process, at 1,000× and 10,000× magnification.*

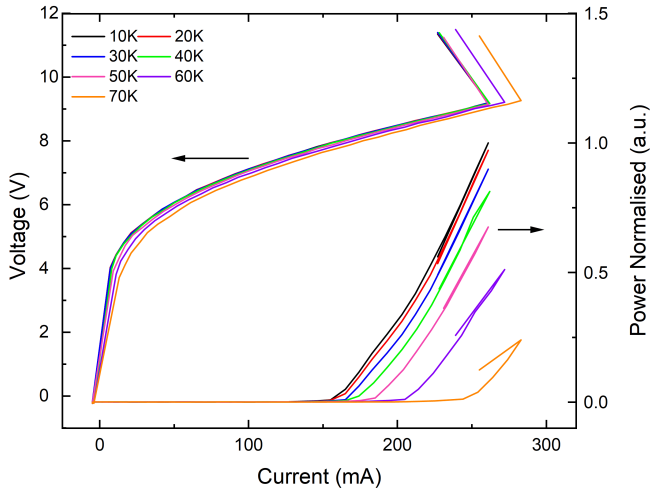

Fig 3 *Light–current–voltage measurements of the 4.7-THz waveguide-integrated QCL at a 2% duty cycle between* 10 K - 70 K.

area and wire-bonded to an integrated electrical SMA connector via an intermediate thermal-isolation heatsink, prior to final assembly of the waveguide module.

Device characterisation: The QCL was mounted on the cold-finger of a Janis ST-100 liquid-helium cryostat, and driven using an Agilent 8114A high-current pulse generator (2% duty cycle; 10 kHz repetition rate). This current pulse train was externally gated using a 167-Hz square-wave envelope, and the emitted THz radiation was coupled into a helium-cooled bolometric detector using a pair of off-axis paraboloidal mirrors. A lock-in amplifier, referenced to the pulse envelope, was used to record the bolometric signal as a function of QCL drive current, as shown in Figure 3. A threshold current of 160 mA was observed at low heatsink temperatures, and a maximum operating temperature of 70 K was determined, indicating successful optical integration and outcoupling from the waveguide module.

The emission spectrum of the QCL was recorded using a Bruker Fourier Transform Infrared (FTIR) spectrometer, at a range of drive currents, as shown in Figure 4. Multimode emission was observed, with principal lines seen at 4.749 THz, 4.789 THz and 5.010 THz.

The potential for operation at high duty cycle (or continuous wave) was assessed by recording the peak output power of the laser, as a function of the duty cycle of the power supply, with the QCL operating at a bias of 250 mA. Figure 5) shows that the emitted THz power decreases as duty-cycle increases, owing to internal Joule heating within the QCL active region. Nevertheless, emission is achieved up to 90% duty cycle at 10 K.

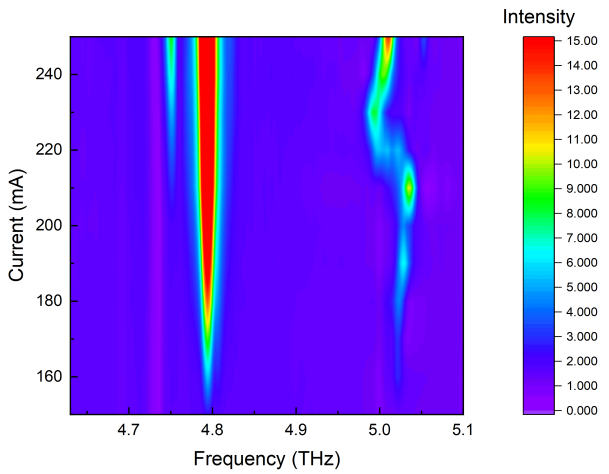

Fig 4 *FTIR spectrum of the waveguide-integrated QCL at a range of drive currents.*

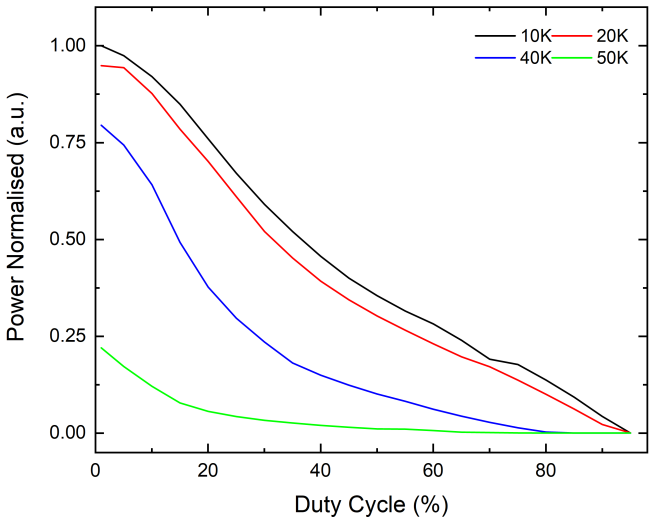

Fig 5 *Output power of the waveguide integrated QCL as a function of duty cycle, at a fixed bias of* 250 mA. *Results are shown for a range of heatsink temperatures.*

The difference between the internal temperature of the QCL active region T_{QCL} and the measured heatsink temperature T_{HS} can be approximated by a linear thermal resistance model:

$$\Delta T = T_{QCL} - T_{HS} \approx IV\gamma R_{th} \quad (1)$$

where I is the peak QCL drive current, V is the voltage dropped across the laser, γ is the duty cycle, and R_{th} is the thermal resistance between the QCL active region and the heat sink.

At low duty cycles, Joule heating is negligible, and therefore $T_{QCL} \approx T_{HS}$. As such, the low duty-cycle output power in Figure 3 may be used as a thermometric property, allowing the internal temperature of the QCL to be inferred at higher duty cycles from Figure 5.

The thermal resistance between the QCL and the heatsink was calculated as 31 K/W, at 10 K heat-sink temperature and at a drive current of 250 mA. As a result, a d.c. bias on the QCL leads to an inferred internal temperature of $T_{QCL} \approx 90$ K, which exceeds the maximum operating temperature of the device. Improvements in the solder-mounting between the QCL and the waveguide module could potentially reduce the thermal resistance and enable continuous-wave operation.

Beam profile analysis: The far-field beam divergence was measured from each feedhorn using a knife-edge technique. The QCL was driven in pulsed mode at a current of 240 mA with an 8% duty-cycle, and at a heat-sink temperature of 10 K to obtain maximal output power. The beam was coupled into a bolometric detector using a pair of paraboloidal mirrors, as described previously.

A knife edge was placed in the divergent part of the QCL emission, at a distance of 110 mm from the feedhorn aperture. The calculated Fraunhofer range was 78 mm for the QCL emission wavelength, and feedhorn aperture size. The power coupled into the detector was recorded as the knife edge was scanned progressively through the beam at 1 mm intervals. This was then differentiated to obtain the profile of the beam, as shown in Figure 6. Repeat measurements were taken with the knife edge moving in the directions parallel and perpendicular to the interface between the two halves of the split-block structure, and for each feedhorn.

A dual-lobed profile was observed for both feedhorns in the perpendicular direction, whereas the parallel profile was almost single-lobed. Although a diagonal horn is expected to yield a single-lobed emission, the split-block geometry induces a conductivity defect in the perpendicular direction, and hence a phase shift in the near-field. At >4.7 THz, the size of this defect may be significant enough to result in a splitting of the far-field pattern, offering a potential explanation for the observed anomalous pattern.

The angles of divergence of the front diagonal feedhorn was 4.5° and 4.9° in the perpendicular and parallel directions respectively. A value of 6.0° in the parallel direction of the back diagonal feedhorn was cal-

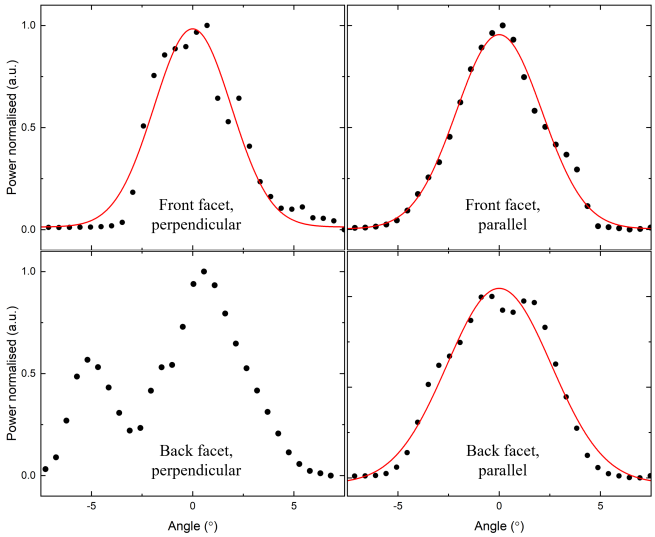

Fig 6 *Derivative plot of the knife edge measurements of the front facet (top) and back facet (bottom) in the perpendicular plane (left) and parallel plane (right) of the waveguide block.*

culated. The perpendicular profile showed strong dual-lobed behaviour and therefore the angle of divergence is poorly defined. These values are somewhat larger than the analytical value calculated for a uniform field across a square aperture, 2.9°, indicating that the near field is confined to a narrower region within the aperture. The larger back-feedhorn divergence in both planes, is likely to be a combination of alignment of the QCL within the waveguide and resulting differences in the near-field mode, and experimental uncertainty in the measurement of the knife-edge distance from the feedhorn.

As QCL emission results from intersubband transitions, the polarisation is expected to be linear. However, an ellipticity of $R = 1.6$ was determined from a measurement of the front feedhorn using a pair of Microtech G50 wire-grid polarizers, implying that the waveguide structure results in some depolarisation of the QCL beam.

Conclusion: We have demonstrated the successful fabrication and integration of a >4.7-THz QCL into a waveguide cavity—the highest frequency waveguide integrated THz QCL to date. A reduction in surface-roughness in the external waveguide structure was achieved through diamond-turning and electro-less plating, enabling pulsed QCL operation up to 70 K, or up to 90% duty cycle at low temperature. A low beam divergence was observed, on the scale of <5°, matching the level achievable with complex facet-patterning techniques. However, the dual-lobed emission profile may introduce challenges for far-field coupling to external devices. Future work will be on improvements in thermal management, and in feedhorn design to achieve single-lobed, continuous-wave emission.

Funding information: This work has been supported by UK Research and Innovation (Future Leaders Fellowship MR/S016929/1), the European Space Agency (General Support Technology Programme contract 4000114487/15/NL/AF), the UK Space Agency (contract NSTP3-FT2-002), the Centre for Earth Observation Instrumentation (Fast Track contract RP10G0435A03), the Royal Society (Wolfson Research Merit Award WM150029) and the Engineering and Physical Sciences Research Council (Programme grant EP/P021859/1)

Conflict of interest: The authors have declared no conflict of interest.

Data availability statement: The data that support the findings of this study are openly available in the Research Data Leeds repository at https://doi.org/10.5518/1141, reference number [reference number].

References

1. Köhler, R., et al.: Terahertz semiconductor-heterostructure laser. Nature 417, 156–159 (2002). https://doi.org/10.1038/417156a
2. Hübers, H.W., et al.: Terahertz quantum cascade laser as local oscillator in a heterodyne receiver. Opt. Express 13(15), 5890–5896 (2005). https://doi.org/10.1364/OPEX.13.005890
3. Dean, P., et al.: Absorption-sensitive diffuse reflection imaging of concealed powders using a terahertz quantum cascade laser. Opt. Express 16(9), 5997–6007 (2008). https://doi.org/10.1364/OE.16.005997
4. Kim, S.M., et al.: Biomedical terahertz imaging with a quantum cascade laser. Appl. Phys. Lett. 88, 153903 (2006). https://doi.org/10.1063/1.2194229
5. Adam, A.J.L., et al.: Beam patterns of terahertz quantum cascade lasers with subwavelength cavity dimensions. Appl. Phys. Lett. 88(15), 151105–151105–3 (2006). https://doi.org/10.1063/1.2194889
6. Miao, W., et al.: Demonstration of a fully integrated superconducting receiver with a 2.7 thz quantum cascade laser. Opt. Express 23, 4453–4458 (2015). https://doi.org/10.1364/OE.23.004453
7. Wanke, M.C., et al.: Monolithically integrated solid-state terahertz transceivers. Nat. Photonics 4(8), 565–569 (2010). https://doi.org/10.1038/nphoton.2010.137
8. Kundu, I., et al.: Terahertz photonic integrated circuit for frequency tuning and power modulation. Opt. Express 28(4), 4374–4386 (2020). https://doi.org/10.1364/OE.380656
9. Valavanis, A., et al.: Mechanically robust waveguide-integration and beam shaping of terahertz quantum cascade lasers. Electron. Lett. 51(12), 919–921 (2015). https://ddoi.org/10.1049/el.2015.1137
10. Ellison, B.N., et al.: 3.5 thz quantum-cascade laser emission from dual diagonal feedhorns. Int. J. Microwave Wireless Technol. 11, 909–917 (2019). https://doi.org/10.1017/S175907871900028X
11. Richter, H., et al.: Direct measurements of atomic oxygen in the mesosphere and lower thermosphere using terahertz heterodyne spectroscopy. Commun. Earth Environ. 2(1), 1–9 (2021). https://doi.org/10.1038/s43247-020-00084-5
12. Schrottke, L., et al.: Quantum-cascade lasers as local oscillators for heterodyne spectrometers in the spectral range around 4.745 THz. Semicond. Sci. Technol. 28(3), 035011 (2013). https://doi.org/10.1088/0268-1242/28/3/035011
13. Johansson, J.F., Whyborn, N.D.: The diagonal horn as a sub-millimeter wave antenna. IEEE Trans. Microw. Theory Techniques 40(5), 795–800 (1992). https://doi.org/10.1109/22.137380
14. Tonouchi, M.: Cutting-edge terahertz technology. Nat. Photonics 1, 97–105 (2007). http://doi.org/10.1038/nphoton.2007.3
15. Yu, N., et al.: Designer spoof surface plasmon structures collimate terahertz laser beams. Nat. Mater. 9(9), 73–735 (2010). https://doi.org/10.1038/nmat2822
16. Scalari, G., et al.: Far-infrared ($\lambda \approx 87\,\mu$m) bound-to-continuum quantum-cascade lasers operating up to 90 K. Appl. Phys. Lett. 82(19), 3165–3167 (2003). https://doi.org/10.1063/1.1571653
17. Li, L., et al.: Terahertz quantum cascade lasers with >1 W output powers. Electron. Lett. 50(4), 309–311(2) (2014). https://doi.org/10.1049/el.2013.4035
18. Sevin, G., et al.: Continuous-wave operation of 2.7 THz photonic crystal quantum cascade lasers. Electron. Lett. 46(22), 1513 –1515 (2010). https://doi.org/10.1049/el.2010.2036
19. Amanti, M.I., et al.: Horn antennas for terahertz quantum cascade lasers. Electron. Lett. 43(10), 573–574 (2007). https://doi.org/10.1049/el:20070450
20. Lee, A.W.M., et al.: High-power and high-temperature THz quantum-cascade lasers based on lens-coupled metal-metal waveguides. Opt. Lett. 32(19), 2840–2842 (2007). https://doi.org/10.1364/OL.32.002840
21. Amanti, M.I., et al.: Low-divergence single-mode terahertz quantum cascade laser. Nat. Photonics 3(10), 586–590 (2009). https://doi.org/10.1038/nphoton.2009.168
22. Williams, B.S.: Terahertz quantum-cascade lasers. Nat. Photonics 1, 517–525 (2007). https://doi.org/10.1038/nphoton.2007.166
23. Wienold, M., et al.: High-temperature, continuous-wave operation of terahertz quantum-cascade lasers with metal-metal waveguides and third-order distributed feedback. Opt. Express 22(3), 3334–3348 (2014). https://doi.org/10.1364/OE.22.003334
24. Williams, B.S., et al.: Terahertz quantum-cascade laser at $\lambda \approx 100\,\mu$m using metal waveguide for mode confinement. Appl. Phys. Lett. 83(11), 2124–2126 (2003). https://doi.org/10.1063/1.1611642
25. Wienold, M., et al.: Frequency dependence of the maximum operating temperature for quantum-cascade lasers up to 5.4 THz. Applied Physics Letters 107(20), 202101 (2015). https://doi.org/10.1063/1.4935942